Light scattering in a magnetically polarizable nanoparticle suspension

Article *in* Physical Review E · October 2008

DOI: 10.1103/PhysRevE.78.031404 · Source: PubMed

3 authors:

Junaid Masud Laskar
Max Planck Institute for Dynamics and Self-O…
14 PUBLICATIONS **231** CITATIONS
SEE PROFILE

John Philip
Indira Gandhi Centre for Atomic Research
199 PUBLICATIONS **4,220** CITATIONS
SEE PROFILE

Baldev Raj
Indira Gandhi Centre for Atomic Research
880 PUBLICATIONS **9,074** CITATIONS
SEE PROFILE

Light scattering in a magnetically polarizable nanoparticle suspension

Junaid M. Laskar, John Philip,* and Baldev Raj
SMARTS, NDED, Metallurgy and Materials Group, Indira Gandhi Centre for Atomic Research, Kalpakkam 603 102, Tamilnadu, India
(Received 6 June 2008; revised manuscript received 13 August 2008; published 10 September 2008)

We investigate magnetic-field-induced changes on transmitted light intensity in a magnetic disordered phase of iron oxide nanoparticle suspension. We observe a dramatic decrease in the transmitted light intensity at a critical magnetic field. The critical magnetic field follows power-law dependence with the volume fraction of the nanoparticles suggesting a disorder-order structural transition. The light intensity recovers fully when the magnetic field is switched off. We discuss the possible reasons for the reduction in the light intensity under the influence of magnetic field. Among the various mechanisms such as Kerker's condition for zero forward scattering, Faraday effect, Christiansen effect, photoinduced refractive index mismatch between the two components of the dispersion, etc., the resonances within the magnetic scatterers appear to be the plausible cause for the extinction of light. The circular pattern observed on a screen placed perpendicular to the incident beam confirms the formation of rodlike structures along the direction of propagation of the light.

DOI: 10.1103/PhysRevE.78.031404 PACS number(s): 82.70.Dd, 64.70.Nd

I. INTRODUCTION

Colloids are wonderful model systems for many fundamental studies [1]. For example, the pioneering demonstration of the fractal nature of clusters in colloidal suspension [2] has triggered interest in the limits of gelation, rheology, sedimentation, pattern formation, etc. The observation of long-range orientational distortions around colloidal particles in liquid crystalline matrices opened up a new fascinating field of research [3]. Similarly, the phase behavior of mixed colloidal systems has been a topic of intense interest for quite some time [4]. Among colloidal systems, magnetically polarizable particles are distinct because they are easy to manipulate with applied magnetic field and hence they are ideal candidates for many fundamental studies and practical applications [5–9]. Combined use of neutron polarization with small-angle scattering has been used to get insight into the structure of the ferrofluid in an applied magnetic field [10]. The existence of nematic type ordering in ionic ferrofluids was confirmed by optical and x-ray scattering [11]. The small-angle neutron scattering (SANS) and small-angle x-ray scattering (SAXS) measurements on dilute ferrofluid dispersed in soft polymer gels show that the particles in the fluid form fractal aggregates. They orient in the presence of a magnetic field and are restricted in both their translational and rotational freedom [12]. Monte Carlo studies in ferrofluids show agglomeration probability is higher for the larger particle radius [13]. The field-induced anisotropy studies in ferrofluids using two-dimensional small angle x-ray scattering show that with the application of a homogeneous magnetic field, the nanoparticles form anisotropic clusters with preferred parallel orientation with respect to the applied magnetic field. This study shows that van der Waals interaction yields a significant contribution, and cannot be neglected in polydisperse systems [14]. The structure of ferrofluid at low temperature has been investigated using Monte Carlo simulations. It has been found that extensive particle association into chainlike and ringlike clusters at low density and a progression of fluid structures from the low-density associated phase to the high-density liquid phase leads to a fluid-fluid transition [15]. Very recently, the dynamics of ordering and relaxation processes in magnetic colloids has been studied using a novel stroboscopic small-angle neutron scattering technique in an oscillating magnetic field, which enabled elucidating the dynamical nature of the locally ordered domains in ferrofluids. The alignment of particle moments along the applied field is governed by the fast Brownian rotation of individual nanoparticles and small aggregates, while the magnetic relaxation of longer dipolar chains and local hexagonal domains is much slower [16]. This group has also done extensive studies on the reversal of magnetic moments of nanoparticles in concentrated ferrofluids under an oscillating magnetic field by the time-resolved stroboscopic small-angle neutron-scattering technique [17–19].

On increasing the amount of scattering beyond a critical value, the material undergoes a transition into a localized state because of interference of all the scattered waves. Under this condition, the standard radiative transport and diffusion theory to describe the wave propagation through a random medium becomes inadequate. A disorder-induced phase transition in the electron-transport behavior from the classical diffusion regime to a localized state in which the material behaves as an insulator was predicted by Anderson [20]. The Anderson-localization transition of electromagnetic waves in disordered media has been a topic of intense research during the last few decades [21–37]. The weak localization of an electromagnetic wave leads to a coherent enhancement of light in the backward direction, which has been experimentally observed in several systems such as dense latex microspheres, highly concentrated aqueous suspension of polystyrene particles, submicron sized SiO_2 beads in air, semiconductor microcavity, etc. [24–26]. The diffusion coefficient and absorption length of optical propagation in strongly scattering media of submicron titania crystals randomly distributed in a porous wedged polystyrene matrix has been investigated [29]. The strong photon localization is first observed in random mixtures of metallic and dielectric spheres in the microwave region [30]. In a strongly scatter-

*Corresponding author. philip@igcar.gov.in

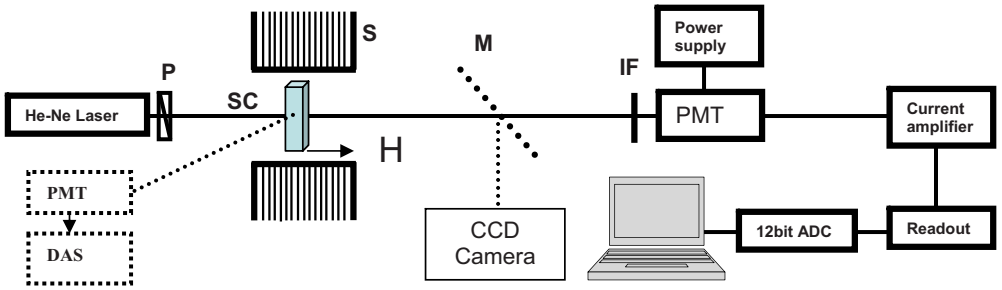

FIG. 1. (Color online) Schematic of the experimental setup. The direction of the applied magnetic field is along the direction of propagation of the beam. P, polarizer; SC, sample cuvette; S, solenoid; M, mirror; PMT, photomultiplier tube; DAS, data acquisition system (for backscattering intensity measurement); and IF, interference filter.

ing medium, the velocity for an electromagnetic wave may differ from the phase velocity and the group velocity [31]. A macroscopic derivation of the speed of light relevant from the energy transport in media containing randomly distributed scatterers has been derived [32]. A transverse diffusive current in a Faraday active disordered dielectric medium was predicted and realized experimentally [33]. The coherent backscattering of light was observed in nematic liquid crystals and suspension of TiO_2 [34,35]. Direct experimental evidence for Anderson localization of light in very strongly scattering semiconductor (GaAs) powders, tunable light localization effects in liquid crystal photonic band-gap materials, and weak localization of light in a disordered semiconductor microcavity have been realized [36,37].

The study of diffusion processes in a magnetic colloid by a forced Rayleigh scattering technique under an applied static field showed a periodic spatial modulation of particle concentration (transient grating) under different field geometries [38,39]. A dynamic light scattering study of ferrofluid particles subjected to a magnetic field reveals that the effective diffusion coefficient has a pronounced dependence on the scattering wave vector q, reflecting two modes of motion: translational diffusion of the whole chain, and fluctuations of particles within a chain [40]. Based on the analogy to polymer chain dynamics, they attribute these behaviors to the contribution of hydrodynamic interactions that couple particle motion within a chain. A dramatic increase of the optical attenuation along the field direction was observed in a suspension of magnetic particles [41]. The photonic Hall effect in liquid and gelled samples of ferrofluids has been studied both experimentally and theoretically [42]. The phenomena of scattering and diffraction of light in magnetic suspensions and emulsions and mixtures of magnetic and nonmagnetic scatterers have been investigated [43–52]. Vanishing of both forward and backward scattered laser light from a dispersion of micron-sized magnetic particles in a ferrofluid, above some critical magnetic field, has been reported [43,44]. A systematic study in model ferrofluid emulsion subjected to a slowly increasing magnetic field showed a complicated structural behavior from a gas of Brownian particles to columnar solid structures [45]. They also observed two intermediate structural transitions: (i) randomly distributed chains and particles and (ii) distinct thin columns and randomly distributed chains and particles.

There have been studies on scattering of light in magnetic scatterers, in the size limit of $a \gg \lambda$ [43–45,50–52]. However, scattering in the limit $a \ll \lambda$ is still an unexplored area, probably due to practical limitations to tailor stable and monodispersed model suspensions [53]. Here, a is the scatterer size and λ is the wavelength of light. The aim of this paper is to investigate the effect of applied magnetic field on transmitted light intensity in a magnetically disordered medium where the suspended particle size is less than the incident light wavelength. The questions we address from these studies are (i) Can the light intensity be reversibly tuned with an external magnetic field? (ii) Can the light be made extinct at a critical magnetic field? (iii) What is the mechanism responsible for such extinction of light?

II. EXPERIMENTAL SECTION

The suspension used in our studies was a disordered magnetic medium where the particle size is less than the incident light wavelength ($a < \lambda$) [53]. We measure both the forward and backward scattered light intensity as a function of applied magnetic field. We used a stable colloidal suspension of magnetite (Fe_3O_4) nanoparticles of average diameter 6.7 nm, coated with oleic acid and dispersed in kerosene. The organic layer thickness around the particles is about 1.5 nm. The polydispersity index is measured by dynamic light scattering using a Nano ZS apparatus, Malvern Instrument. The polydispersity index (PDI) accounts the relative error between curve fit and experimental values. A suspension with a PDI value lower than 0.1 is considered as fairly monodisperse. The polydispersity index of our sample was 0.092. The suspensions used in our experiments had excellent long-term stability with no agglomerations even after prolonged application of very strong magnetic fields.

The experimental setup is shown in Fig. 1. The ferrofluid sample is taken in a quartz cuvette and kept inside a solenoid, where magnetic field is varied by changing the current passing through its coil using a dc power supply. The direction of magnetic field is parallel to the light propagation. An amplitude and frequency stabilized polarized He-Ne laser (Spectra-physics) of wavelength 632.8 nm with an output power 1 mW is used as a light source. The light intensity is measured by using a photomultiplier tube (PMT) (Oriel). The output of the PMT is fed to readout through a current amplifier with variable gain. The analog output from the readout is connected to a 12 bit analog-to-digital converter (ADC) that is interfaced with a computer. For observation,

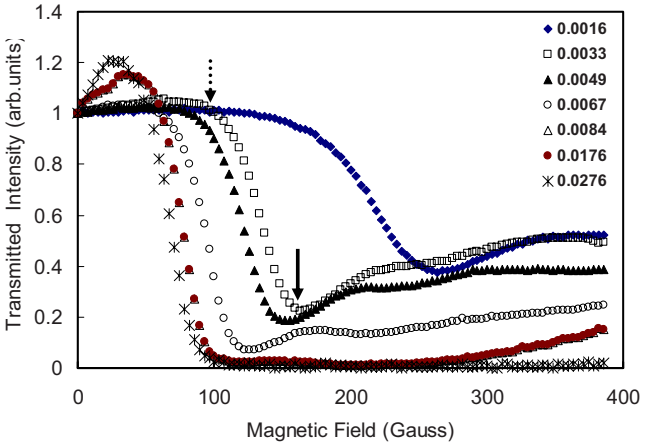

FIG. 2. (Color online) Normalized forward transmitted light intensity as a function of applied magnetic field for magnetite-based ferrofluid of different volume fractions. The average particle diameter was 6.7 nm.

the scattered light from the sample is projected on a screen and recorded using a charge coupled device (CCD) camera. The backscattering experimental geometry is shown by dotted lines. The transmitted light intensity through the sample has been acquired as a function of external magnetic field. The variation in the magnetic field within the sample was less than 1% and the variation within the laser spot diameter was less than 0.01%.

III. EXPERIMENTAL RESULTS AND DISCUSSION

A. Light intensity in forward and backward direction

Figure 2 shows the normalized transmitted intensity as a function of external field for different magnetite volume fractions. The intensity plotted was the ratio of the intensity transmitted through the sample with and without magnetic field. Here, at lower concentrations, the transmitted light intensity remains constant up to a "critical" magnetic field H_{C1}, above which the intensity starts to decrease drastically. At another "critical" magnetic field called H_{C2} the transmitted light intensity becomes a minimum. For 0.0033 volume fraction, H_{C1} and H_{C2} are shown by the dotted and solid arrow, respectively. Above H_{C2}, the transmitted light intensity increases slowly.

To assess the effect of volume fraction of nanoparticles on the critical magnetic field, we plot the variation of the critical fields H_{C1} and H_{C2} as a function of volume fraction of the nanoparticles in Fig. 3. Both H_{C1} and H_{C2} follow power-law decay with volume fraction ($H_C \propto \phi^{-x}$) where the exponents are 0.423 and 0.283, respectively. The scaling analysis also predicts such power-law dependence where exponents can vary between 0.25 and 0.75 for structural transitions in ferrofluid emulsion under external magnetic field [45]. Also, with increasing concentrations, the slope of the transmitted intensity curve (between H_{C1} and H_{C2}) increases. At higher particle concentrations, i.e., above 0.0176 volume fraction, the transmitted light intensity at first increases slightly and then decreases with increasing magnetic field.

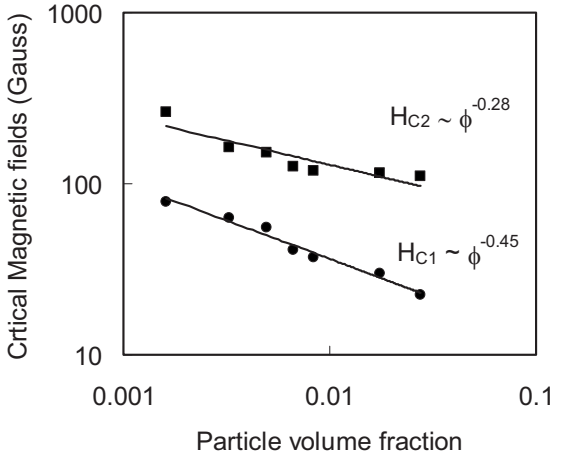

FIG. 3. Critical magnetic fields (H_{C1} and H_{C2}) as a function of magnetite volume fraction. The critical fields H_{C1} and H_{C2} follow power-law decay with volume fraction ($H_C \propto \phi^{-x}$) where the exponents are 0.423 and 0.283, respectively. Reprinted with permission from [53]. Copyright 2008, American Institute of Physics.

Figure 4 shows the transmitted intensity of light in the forward and backward directions as a function of external field for a volume fraction of 0.0067. It can be seen that both the forward and backward intensity drops to a minimum at the same magnetic field.

B. Effect of polarization on transmitted light intensity

The experiments are repeated using laser light of different polarizations. We used a linearly polarized (vertical and horizontal) light beam and a circularly polarized light. In all the above experiments, we have obtained similar results. The normalized transmitted light intensity using vertical, horizontal, and circular polarization of light is plotted in Fig. 5.

C. Forward scattering patterns at different magnetic fields

The forward scattering patterns from a magnetite suspension of 0.0067 volume fraction at various magnetic fields are shown in Fig. 6. Here, the transmitted light intensity drops to

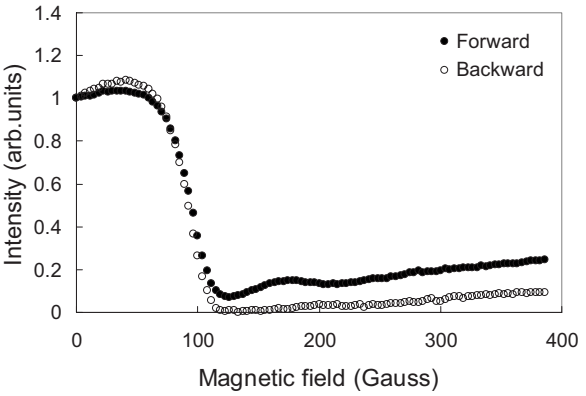

FIG. 4. Normalized forward and backward scattered light intensity as a function of applied magnetic field for ferrofluid of 0.0067 volume fraction.

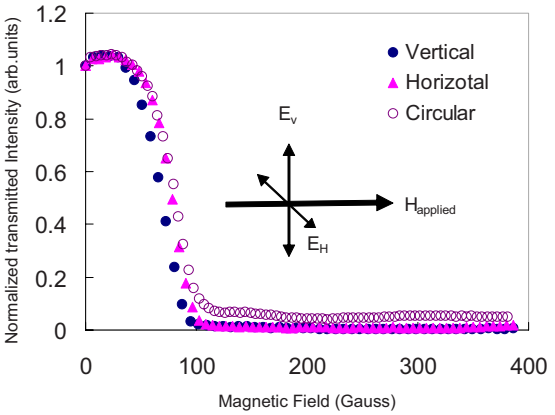

FIG. 5. (Color online) Normalized transmitted light intensity using vertical (E_V) horizontal (E_H), and circular polarization of light as a function of applied magnetic field ($H_{applied}$).

zero at a magnetic field strength of 115 G, above which the forward scattered light shows a diffused ringlike structure, i.e., when the applied magnetic field is above H_{C2}. The ring becomes sharper as the magnetic field strength increases. It should be noted that the spots are occurring at the same place at different magnetic fields. However, the spot size decreases as the magnetic field strength increases.

We have also performed an experiment to look at the Faraday rotation effect on the observed extinction of light. Here, the sample was placed between crossed polarizers and the transmitted intensity is plotted as a function of magnetic field strengths. The maximum Faraday shift obtained in our sample was less than 1.5°. The obtained results were consistent with the values reported in the literature [54]. This shows that the intensity variations due to Faraday rotation do not play a major role on the intensity variations plotted as a function of magnetic field.

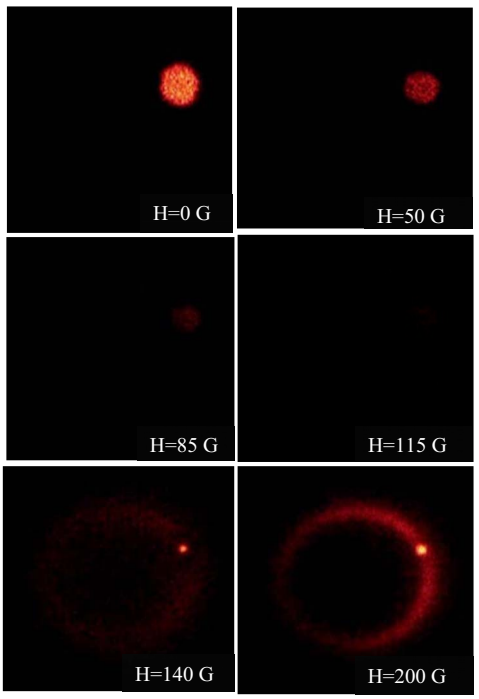

FIG. 6. (Color online) Forward scattered patterns from ferrofluids of 0.0067 volume fraction at various magnetic fields: (a) 0, (b) 50, (c) 115, (d) 140, and (e) 200 G. The transmitted light intensity starts to decrease above 50 G and is fully extinct at 115 G cabove which the forward scattered light shows a diffused ringlike structure.

D. Structural changes in the presence of magnetic field

What happens to the magnetic nanoparticles in the suspension when the external magnetic field is applied? The magnetite nanoparticles in suspension acquire dipole moments in the presence of external magnetic field. The magnitude of the induced dipole moment of an individual nanoparticle is given by [55]

$$m = \frac{\pi}{6} a^3 \chi H_0, \tag{1}$$

where a is the diameter of the nanoparticles, χ is the effective susceptibility of an individual nanoparticle and H_0 is the magnitude of the external magnetic field. The anisotropic interaction energy U_{ij} between two identical parallel point dipoles with magnitude m is given by [56]

$$U_{ij}(r_{ij}, \theta_{ij}) = \frac{m^2 \mu_0}{4\pi} \left(\frac{1 - 3\cos^2 \theta}{r_{ij}^3} \right), \tag{2}$$

where μ_0 is the parameter symbolizing magnetic permeability of free space, r_{ij} is the magnitude of the vector describing the distance between the centers of the ith and jth nanoparticles and θ_{ij} is the angle between the vector $\mathbf{r}_{ij}$ and the external field vector. The effective magnetic interaction between two magnetic nanoparticles can be described by the coupling constant

$$L = -\frac{U(a,0)}{K_B T} = \frac{\pi \mu_0 a^3 \chi^2 H_0^2}{72 K_B T}. \tag{3}$$

Coupling constant is the ratio of the maximum magnitude interaction energy to the thermal energy ($k_B T$) in the system. Here k_B is the Boltzmann constant and T is the temperature. The nanoparticles in the magnetic suspension will self-assemble into structures aligned with the external magnetic field when $L \gg 1$.

Without any external magnetic field the magnetic moments of the scatterers are oriented in random directions. With the increase in magnetic field the moments of the magnetic particles start to align themselves along the direction of the magnetic field. The lengths of the chains increase with increasing magnetic field until the path length of the sample cell. The *in situ* cryogenic transmission electron microscopic observations of magnetite nanoparticles dispersions under magnetic field confirm columnar structures exhibiting distorted hexagonal symmetry [18]. In the absence of any magnetic field these structures were distorted by lens-shaped voids due to weak dipole-dipole attraction. In addition such field-induced ordering is observed in aqueous ferrofluids [52].

E. Possible reasons for extinction of light

What are the possible reasons for the observed extinction of light at H_{C2}? The absorption study in kerosene-based ferrofluid in the visible range (400–800 nm) shows no characteristic visible absorption peak around 632 nm (for particle size of 10 nm, $\phi=0.036$; for path length 10 mm the absorbance was 0.015) [57]. As the wavelength of the laser light that is used for the experiment is 632.8 nm and the volume fraction was much lower than the above case, the extinction of light cannot be due to absorption. Of course there is no reason for the light to absorb at a feeble magnetic filed strength of 0.02 T. Therefore, this possibility is also ruled out. Similarly the magnetic field destroys the time reversal symmetry on which the occurrence of weak and strong localization relies [27]. Can this be due to the dynamics of nanoparticles during the field-induced ordering? In ferrofluids nanoparticles are usually smaller than domain size and are free to rotate independently from each other. Brownian motion and Neel rotation are relaxation mechanisms due to particle and spin rotation, respectively [17]. For a particle of 10 nm size, the values of τ_N and τ_B are 10^{-9} and 7.6×10^{-7} s, respectively. However, the value of τ_N increases sharply with the size of the particle due to the exponential dependence on V'. The time dependent transmission measurement at a different rate of application of magnetic fields shows 100–180 s for a complete recovery from the extinction. Therefore, the internal dynamics should not be the root cause for the observed extinction.

Another mechanism for the decrease of transmitted light is the optical limiting of laser light from a colloidal suspension of spherical particles [58]. This limiting has been shown to be mainly due to nonlinear light scattering by the two-component colloidal suspension system. However, such enhanced nonlinear light scattering takes place only at high fluences due to the photoinduced mismatch of the refraction indices of the two components in colloidal suspension. Since the incident laser light intensity is very small (1 mW), the above-mentioned possibility of nonlinear light scattering due to photo-induced refractive index mismatch between the two components of the suspensions can be ruled out.

Christiansen has shown that in small grains of particle suspensions, the dispersion curves can coincide at one wavelength [59,60]. However, at 632.8 nm, the refractive indices of dispersed (magnetic nanoparticles) and dispersion medium (kerosene) do not coincide. Therefore the possibility of the decrease of light due to the Christiansen effect is also ruled out. Kerker's theory deals with the scattering of light by magnetic spheres [46]. Considering magnetic permeability $\mu\neq1$ in the small particle (or long wavelength) limit, the two polarized components of scattered radiant intensity with electric vectors perpendicular and parallel to the scattering plane due to the incidence of a plane wave of unit irradiance and wavelength λ in an isotropic homogeneous sphere of radius a and refractive index m are derived [46].

According to Kerker's theory, when $\varepsilon=\frac{(4-\mu)}{(2\mu+1)}$, $I_1(0^0)=I_2(0^0)=0$. This means that both the components of forward scattered intensity become zero. Is it possible to fulfill Kerker's condition for zero forward scattering at $a\ll\lambda$, as suggested recently [43,44]? The light that is incident and gets scattered from the Fe_3O_4 nanoparticles is in the visible range of the spectrum (wavelength $\lambda=632.8$ nm) and hence the magnetic permeability value $\mu=1$. Since Kerker's condition [Eq. (16)] is derived for frequencies lower than optical frequency, it cannot be applied in our case.

Then, what could be the reason for the observed extinction? For a disordered medium of identical scatterers of radius a, illuminated by light of wavelength λ, the localization parameter $k\ell^*$ depends on the scatterer's magnetic permeability μ_S, where $k=\frac{2\pi}{\lambda}$ is the wave vector and $\ell^*=\frac{\ell}{(1-\langle\cos\theta\rangle)}$ is the transport mean-free path [33,47]. The anisotropy factor $\langle\cos\theta\rangle$ and photon mean-free path $\ell=\frac{1}{(\Phi\sigma)}$ can be expressed as the functions of the Mie coefficients a_n and b_n [33,47]. Here, Φ is the number density of scatterers and σ is the total scattering cross section, $\sigma=(\lambda^2/2\pi)\Sigma_{n=1}^{\infty}(2n+1)\mathrm{Re}(|a_n|+|b_n|)$. In the small particle limit, for magnetic scatterers, $|m|ka\gg1$, as $|\mu|\gg1$.

The anisotropy factor for the lowest order term in ka is

$$\langle\cos\theta\rangle=\frac{\mathrm{Re}(a_1b_1^*)}{(|a_1|^2+|b_1|^2)}. \tag{4}$$

The periodic function $p(m,ka)=ka\tan(mka)$, which depends on magnetic permeability μ, is responsible for the resonances in $\langle\cos\theta\rangle$. By numerical means also the appearance of such resonances in $\langle\cos\theta\rangle$ in the small particle limit ($ka\ll1$) for magnetic scatterers ($\mu\neq1$) are shown [47]. The presence of these resonances leads to an oscillatory behavior of localization parameter $k\ell^*$ with μ. Thus in the small particle limit, each single scattering event is characterized by the presence of forward-backward asymmetry and resonance effects leading to a reduction of transport mean-free path and hence the localization parameter. Is the decrease in the localization parameter in the small particle limit for magnetic scatterers ($\mu\neq1$) responsible for the observed extinction of light? In the present experimental case, as the scattering of light takes place in the visible range of the spectrum, the scatterer magnetic permeability μ should be equal to unity. Therefore the possibility of the decrease of transmitted light intensity due to the above-mentioned mechanism can be ruled out.

As the magnetic field is increased, the sizes of scatterers will increase due to the formation of doublets, triplets, or very small chains, which changes the scatterers' sizes, i.e., the ka value drastically. Considering single scattering, the scattering anisotropy factor $\langle\cos\theta\rangle$ for spheres and extinction efficiency factor Q_{ext} for cylinders as a function of size parameter ka are analyzed in detail [61,62].

Figure 7 shows the variation of scattering anisotropy factor $\langle\cos\theta\rangle$ as a function of size parameter ka for three different values of the magnetic permeability (μ) of the scatterer. Since we deal with scattering at optical frequency, the variation in $\langle\cos\theta\rangle$ for $\mu=1$ is analyzed in detail. For this case, the appearance of resonances in $\langle\cos\theta\rangle$ is observed as ka increases above some limit.

Another important quantity of interest in single scattering is the extinction efficiency factor, Q_{ext}, which is defined as extinction cross section per unit length, c divided by $2a$, the diameter of the cylinder. It represents the fraction of electro-

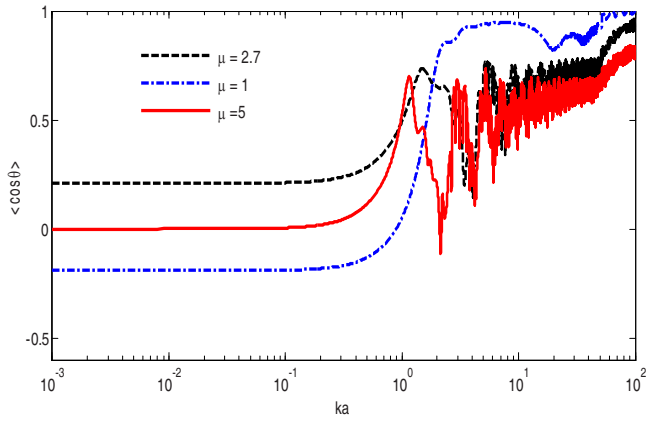

FIG. 7. (Color online) Scattering anisotropy factor $\langle \cos\theta \rangle$ as a function of size parameter ka, for spheres of three different magnetic permeability values 1, 2.7, and 5.

magnetic energy geometrically incident upon the particle that is abstracted from the beam. The extinction efficiency Q_{ext} of a cylinder when the cylinder axis lies in the plane determined by the propagation vector of the incident plane wave k and the electric field E has been derived [62].

Figure 8 shows the behavior of Q_{ext}^{E} as a function of size parameter ka for different incident angles (α) with the cylinder axis for an infinite cylinder with a refractive index 1.6 and magnetic permeability $\mu=1$.

Since the cylindrical structures formed in our dispersion are parallel to the incident light, α is close to zero. One of the interesting results in Fig. 8 is the appearance of a large resonance peak in extinction efficiency factor Q_{ext}^{E} for an incidence angle $\alpha=1°$, at size parameter value $ka=0.663$.

The appearance of resonances in the scattering anisotropy factor $\langle \cos\theta \rangle$ for spheres and extinction efficiency factor Q_{ext}^{E} for cylinders have a strong significance on scattering intensity. Analytically, the resonances in the scattering originate from a sharp minimum in the denominator of the corresponding scattering coefficients. The scattered electromagnetic wave arises from oscillations of electrons in the particle excited by the incident wave and can be imagined to have their origin in density distributions of oscillating electric and magnetic dipoles in the particle [63]. For the scattered electromagnetic wave, the electric wave arises from the electric dipoles and magnetic wave from the magnetic dipoles. The resonances are related to the properties of the individual scattering coefficients, which in turn represent the amplitudes of the electric and magnetic multipoles excited within the particle. Therefore physically the resonances correspond to the resonant excitation of a particular electric or magnetic multipole.

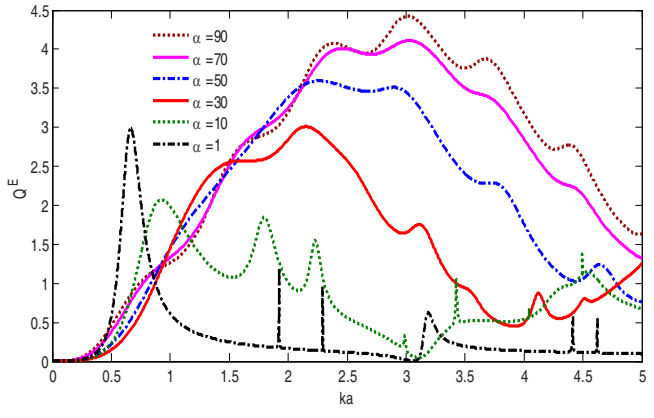

FIG. 8. (Color online) Extinction efficiencies Q_{ext}^{E} as a function of size parameter ka for different incident angles α for an infinite cylinder.

In the absence of any magnetic field, for a wavelength of 632 nm, and particle radius $a=3.35$ nm, the average size parameter (ka) of the particles in the sample is ~ 0.033. As the external magnetic field is increased, the sizes of scatterers will increase due to the formation of doublets, triplets, or very small chains, which changes the scatterers' sizes, i.e., the ka value, drastically. At the critical magnetic field H_{C1}, some of the scatterers' sizes are such that they satisfy the resonances in the scattering anisotropy factor and extinction efficiency factor. At the minimum transmitted intensity, the size distribution is such that the number of scatterers that satisfy the resonance becomes maximum. Therefore the resonances both in the scattering anisotropy factor and extinction efficiency factor, which physically correspond to resonant excitation of a particular electric or magnetic dipole within the scatterer, could be one of the plausible explanations for the observed extinction of light.

F. Origin of ring pattern

What is the reason for the formation of ring structure in the scattered pattern above H_{C2}? The reason for the formation of ring structure on the scattered pattern can be explained by considering scattering of light by a cylinder [61]. It can be shown that light being a physically realizable time-harmonic electromagnetic field ($\mathbf{E},\mathbf{H}$) must satisfy the wave equation

$$\nabla^2\mathbf{E} + k^2\mathbf{E} = 0, \quad \nabla^2\mathbf{H} + k^2\mathbf{H} = 0, \tag{5}$$

where $k^2=\omega^2\varepsilon\mu$, and be divergence-free,

$$\nabla \cdot \mathbf{E} = 0, \quad \nabla \cdot \mathbf{H} = 0. \tag{6}$$

In addition, both the electric field $\mathbf{E}$ and magnetic field $\mathbf{H}$ are dependent on each other

$$\nabla \times \mathbf{E} = i\omega\mu\mathbf{H}, \quad \nabla \times \mathbf{H} = -i\omega\varepsilon\mathbf{E}, \tag{7}$$

where ω is the angular frequency of the electromagnetic wave, k is the wave vector, μ is the magnetic permeability, and ε is the dielectric permittivity of the surrounding medium, respectively. By defining cylindrical vector harmonics in terms of scalar function ψ, also known as the generating function, the vector wave equation (5) can be reduced to the scalar wave equation

$$\nabla^2\psi + k^2\psi = 0, \tag{8}$$

which is expressed in terms of cylindrical coordinates, as scattering from the cylinder is considered. Now, we are interested in evaluating the scattered electromagnetic field when an infinite right circular cylinder of radius a is illuminated by a plane homogeneous wave $\mathbf{E}_i=\mathbf{E}_0 e^{ik\hat{\mathbf{e}}_i\cdot\mathbf{x}}$ propagat-

ing in the direction $\hat{\mathbf{e}}_i = -\sin\zeta\hat{\mathbf{e}}_\mathbf{x} - \cos\zeta\hat{\mathbf{e}}_\mathbf{z}$, where ζ is the angle between the incident wave and the cylinder axis.

There can be two possible orthogonal polarization states of the incident wave depending on whether the electric field is polarized parallel or perpendicular to the xz plane. The expressions for the incident fields for both the polarization states can be expanded in terms of vector cylindrical harmonics. The choice of the radially dependent part of the generating function is based on the finiteness at the origin. Using the orthogonality of cylindrical vector harmonics, the coefficients appearing in the expansion of incident fields are evaluated. Similarly, the scattered electromagnetic fields can also be expanded in vector cylindrical harmonics. The expansion of the scattered fields outside the cylinder is dictated by the continuity of waves at the boundary, the orthogonality of the vector harmonics, and the form of the expansion of the incident fields.

When the incident electric field is parallel to the xz plane, at large distances from the cylinder ($kr\sin\zeta \gg 1$), the scattered field is given by

$$\mathbf{E_S} \sim -E_0 e^{-i\pi/4}\sqrt{\frac{2}{\pi kr\sin\zeta}}e^{ik(r\sin\zeta - z\cos\zeta)} \times \sum_n (-1)^n e^{in\phi}[a_{n\mathrm{I}}\hat{\mathbf{e}}_{\boldsymbol{\varphi}} + b_{n\mathrm{I}}(\cos\zeta\hat{\mathbf{e}}_\mathbf{r} + \sin\zeta\hat{\mathbf{e}}_\mathbf{z})]. \quad (9)$$

Similarly, when the incident electric field is perpendicular to the xz plane, the asymptotic scattered electric field is given as

$$\mathbf{E_S} \sim -E_0 e^{-i\pi/4}\sqrt{\frac{2}{\pi kr\sin\zeta}}e^{ik(r\sin\zeta - z\cos\zeta)}\sum_n (-1)^n e^{in\phi} \times [-a_{n\mathrm{II}}\hat{\mathbf{e}}_{\boldsymbol{\varphi}} - b_{n\mathrm{II}}(\cos\zeta\hat{\mathbf{e}}_\mathbf{r} + \sin\zeta\hat{\mathbf{e}}_\mathbf{z})], \quad (10)$$

where

$$a_{n\mathrm{I}} = \frac{C_n V_n - B_n D_n}{W_n V_n + iD_n^2}, \quad b_{n\mathrm{I}} = \frac{W_n B_n + iD_n C_n}{W_n V_n + iD_n^2}, \quad (11)$$

$$a_{n\mathrm{II}} = -\frac{A_n V_n - iC_n D_n}{W_n V_n + iD_n^2}, \quad b_{n\mathrm{II}} = -i\frac{C_n W_n + A_n D_n}{W_n V_n + iD_n^2}, \quad (12)$$

$$D_n = n\cos\zeta\eta J_n(\eta)H_n^{(1)}(\xi)\left(\frac{\xi^2}{\eta^2} - 1\right), \quad (13)$$

$$A_n = i\xi[\xi J_n'(\eta)J_n(\xi) - \eta J_n(\eta)J_n'(\xi)], \quad (14)$$

$$B_n = \xi[m^2\xi J_n'(\eta)J_n(\xi) - \eta J_n(\eta)J_n'(\xi)], \quad (15)$$

$$C_n = n\cos\zeta\eta J_n(\eta)J_n(\xi)\left(\frac{\xi^2}{\eta^2} - 1\right), \quad (16)$$

$$V_n = \xi[m^2\xi J_n'(\eta)H_n^{(1)}(\xi) - \eta J_n(\eta)H_n^{(1)\prime}(\xi)], \quad (17)$$

$$W_n = i\xi[\eta J_n(\eta)H_n^{(1)\prime}(\xi) - \xi J_n'(\eta)H_n^{(1)}(\xi)], \quad (18)$$

where $\xi = x\sin\zeta$, $\eta = x\sqrt{m^2 - \cos^2\zeta}$, $x = ka$, and also it has been taken $\mu = \mu_1$, $J_n(\rho)$ and $J_n'(\rho)$ are the Bessel function of first kind of integral order n and its derivative with respect to the argument, respectively. $H_n^{(1)}(\rho)$ is the Hankel function of first kind of order n.

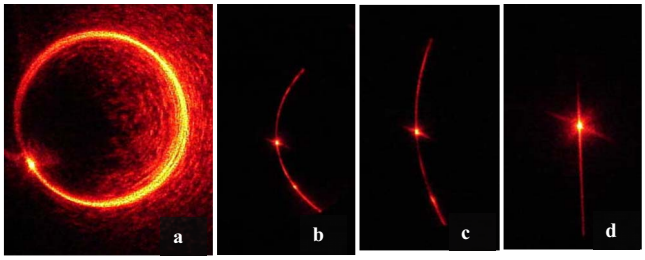

FIG. 9. (Color online) (a)–(d) The scattered wave, on a screen placed perpendicular to the incident beam, from a cylindrical needle (a) parallel, (b) 20°, (c) 45°, and (d) 90°.

From Eqs. (9) and (10) it is clear that the surfaces of constant phase, or wave fronts, of the scattered wave are the points, which satisfy

$$f(x,y,z) = r\sin\zeta - z\cos\zeta = C. \quad (19)$$

Therefore the wave fronts are cones of half-angle ζ with their apexes at

$$z = \frac{-C}{\cos\zeta}. \quad (20)$$

The propagation of the scattered wave can be visualized as a cone that is sliding down the cylinder. The direction of propagation at any point on the cone, or wave normal $\hat{\mathbf{e}}_\mathbf{S}$, is

$$\hat{\mathbf{e}}_\mathbf{s} = \boldsymbol{\nabla} f = \sin\xi\hat{\mathbf{e}}_\mathbf{r} - \cos\xi\hat{\mathbf{e}}_\mathbf{z}. \quad (21)$$

The Poynting vector is therefore in the direction of $\hat{\mathbf{e}}_\mathbf{S}$.

Therefore from the above two equations it is clear that if a screen perpendicular to the incident beam is placed at some distances from the cylinder, the resulting patterns that form on the screen will be conic sections. When the incident light is normal to the cylinder axis, the pattern will be a straight line. As the angle (ξ) between the incident wave and the cylinder (ξ) approaches 0°, the pattern becomes a circle. The formation of the ring clearly establishes the formation of such rodlike structures along the direction of propagation of the light wave above $\mathrm{H_{C2}}$, where the coupling constant $L \geqslant 1$.

The diffused ring at lower magnetic fields indicates the distorted columns due to weak magnetic dipolar attraction. As the magnetic field increases, both the average chain length and the chain number increases. At higher fields, the ring becomes sharper indicating the formation of smooth surfaced columns as evident from the hexagonal symmetry [18]. Figures 9(a)–9(d) show the scattered wave on a screen placed perpendicular to the incident beam, from a cylindrical needle (a) parallel, (b) 20°, (c) 45°, and (d) 90°. Figures 10(a) and 10(b) show the scattered waves from the ferrofluid, when the applied magnetic field is parallel and perpendicular to the direction of propagation of the incoming laser light, respectively. Figures 9 and 10 unambiguously confirm the

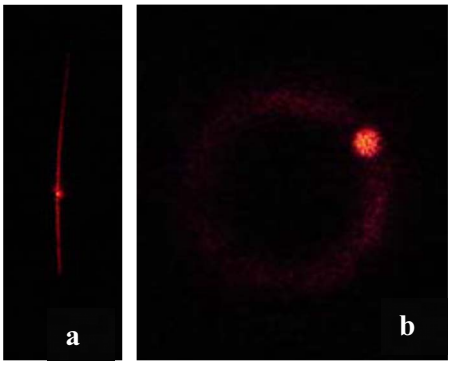

FIG. 10. (Color online) (a) and (b) The scattered waves from the ferrofluid suspension, when the applied magnetic field is (a) parallel and (b) perpendicular to the direction of propagation of the incoming laser light.

presence of a rodlike structure formed in the nanofluid along the field direction, above the second critical magnetic field H_{C2}.

IV. CONCLUSION

We studied the effect of applied magnetic field on transmitted light intensity, in the Mie regime, using magnetite nanoparticles suspensions of different volume fractions. It has been found that irrespective of the polarization of the incoming light beam, extinction of light intensity occurs at a critical magnetic field. Our results confirm the existence of magnetically tunable extinction of light by dilute suspensions of disordered magnetic media ($\sim$3 vol %) in the size limit $a < \lambda$. One of the plausible reasons for the extinction of light is the occurrence of resonances within the scatterers and the subsequent building up of standing waves inside the scatterers that delay the light propagation. However, our results rule out the possibility of absorption, Kerker's condition for zero forward scattering, optical rotation, optical limiting, and Christiansen type effect. The circular patterns observed on a screen placed perpendicular to the incident beam confirm the formation of rodlike structures along the direction of propagation of the light wave above H_{C2}, where the coupling constant $L \geqslant 1$.

ACKNOWLEDGMENTS

We thank Dr. P. R. Vasudeva Rao and Dr. T. Jayakumar for support and encouragement. The authors would like to thank Saji Jacob George for assistance in data acquisition and analysis.

[1] W. B. Russel, D. A. Saville, and W. R. Schowalter, *Colloidal Dispersions* (Cambridge University Press, New York, 1989).
[2] D. A. Weitz, J. S. Huang, M. Y. Lin, and J. Sung, Phys. Rev. Lett. **53**, 1657 (1984).
[3] P. Poulin, H. Stark, T. C. Lubensky, and D. A. Weitz, Science **275**, 1770 (1997).
[4] P. Bartlett, R. H. Ottewill, and P. N. Pusey, Phys. Rev. Lett. **68**, 3801 (1992).
[5] J. Philip, G. Gnana Prakash, T. Jaykumar, P. Kalyanasundaram, and B. Raj, Phys. Rev. Lett. **89**, 268301 (2002).
[6] J. J. Chieh, S. Y. Yang, H. E. Horng, C.-Y. Hong, and H. C. Yang, Appl. Phys. Lett. **90**, 133505 (2007).
[7] H. E. Horng, C. S. Chen, K. L. Fang, S. Y. Yang, J. J. Chieh, C.-Y. Hong, and H. C. Yang, Appl. Phys. Lett. **85**, 5592 (2004).
[8] A. F. Bakuzis, K. Skeff Neto, P. P. Gravina, L. C. Figueiredo, P. C. Morais, L. P. Silva, R. B. Azevedo, and O. Silva, Appl. Phys. Lett. **84**, 2355 (2004).
[9] J. Philip, P. D. Shima, and B. Raj, Appl. Phys. Lett. **91**, 203108 (2007).
[10] R. Pynn, J. B. Hayter, and S. W. Charles, Phys. Rev. Lett. **51**, 710 (1983).
[11] F. M. Da Silva and A. M. Figueiredo Neto, Phys. Rev. E **48**, 4483 (1993).
[12] A. V. Teixeira, I. Morfin, F. Ehrburger-Dolle, C. Rochas, E. Geissler, P. Licinio, and P. Panine, Phys. Rev. E **67**, 021504 (2003).
[13] T. Kruse, A. Spanoudaki, and R. Pelster, Phys. Rev. B **68**, 054208 (2003).
[14] T. Kruse, H.-G. Krauthäuser, A. Spanoudaki, and R. Pelster, Phys. Rev. B **67**, 094206 (2003).
[15] P. J. Camp and G. N. Patey, Phys. Rev. E **62**, 5403 (2000).
[16] A. Wiedenmann, U. Keiderling, M. Meissner, D. Wallacher, R. Gähler, R. P. May, S. Prévost, M. Klokkenburg, B. H. Erné, and J. Kohlbrecher, Phys. Rev. B **77**, 184417 (2008).
[17] A. Wiedenmann, U. Keiderling, K. Habicht, M. Russina, and R. Gahler, Phys. Rev. Lett. **97**, 057202 (2006).
[18] M. Klokkenburg, B. H. Erné, J. D. Meeldijk, A. Wiedenmann, A. V. Petukhov, R. P. A. Dullens, and A. P. Philipse, Phys. Rev. Lett. **97**, 185702 (2006).
[19] M. Klokkenburg, B. H. Erné, A. Wiedenmann, A. V. Petukhov, and A. P. Philipse, Phys. Rev. E **75**, 051408 (2007).
[20] P. W. Anderson, Phys. Rev. **109**, 1492 (1958).
[21] S. John, Phys. Rev. Lett. **53**, 2169 (1984).
[22] S. John, Phys. Rev. Lett. **58**, 2486 (1987).
[23] S. John, Phys. Rev. B **31**, 304 (1985).
[24] Y. Kuga and A. Ishimaru, J. Opt. Soc. Am. A **8**, 831 (1984).
[25] M. P. VanAlbada and A. Lagendijk, Phys. Rev. Lett. **55**, 2692 (1985).
[26] P. E. Wolf and G. Maret, Phys. Rev. Lett. **55**, 2696 (1985).
[27] F. A. Erbacher, R. Lenke, and G. Maret, Europhys. Lett. **21**, 551 (1993).
[28] R. Lenke, C. Eisenmann, D. Reinke, and G. Maret, Phys. Rev. E **66**, 056610 (2002).
[29] A. Z. Genack, Phys. Rev. Lett. **58**, 2043 (1987).
[30] A. Z. Genack and N. Garcia, Phys. Rev. Lett. **66**, 2064 (1991).
[31] M. P. vanAlbada, B. A. vanTiggelen, A. Lagendijk, and A. Tip, Phys. Rev. Lett. **66**, 3132 (1991).
[32] B. A. van Tiggelen, A. Lagendijk, M. P. vanAlbada, and A. Tip, Phys. Rev. B **45**, 12233 (1992).

[33] Bart A. van Tiggelen, Phys. Rev. Lett. **75**, 422 (1995).
[34] H. K. M. Vithana, L. Asfaw, and D. L. Johnson, Phys. Rev. Lett. **70**, 3561 (1993).
[35] R. Sapienza, S. Mujumdar, C. Cheung, A. G. Yodh, and D. Wiersma, Phys. Rev. Lett. **92**, 033903 (2004).
[36] D. S. Wiersma, P. Bartolini, A. Lagendijk, and R. Righini, Nature (London) **390**, 671 (1997).
[37] K. Busch and S. John, Phys. Rev. Lett. **83**, 967 (1999).
[38] J. C. Bacri, A. Cebers, A. Bourdon, G. Demouchy, B. M. Heegaard, B. Kashevsky, and R. Perzynski, Phys. Rev. E **52**, 3936 (1995).
[39] J. C. Bacri, A. Cebers, A. Bourdon, G. Demouchy, B. M. Heegaard, and R. Perzynski, Phys. Rev. Lett. **74**, 5032 (1995).
[40] S. Cutillas and J. Liu, Phys. Rev. E **64**, 011506 (2001).
[41] J. E. Martin, K. M. Hill, and C. P. Tigges, Phys. Rev. E **59**, 5676 (1999).
[42] D. Lacoste, F. Donatini, S. Neveu, J. A. Serughetti, and B. A. Van Tiggelen, Phys. Rev. E **62**, 3934 (2000).
[43] R. V. Mehta, R. Patel, and R. V. Upadhyay, Phys. Rev. B **74**, 195127 (2006).
[44] R. V. Mehta, R. Patel, R. Desai, R. V. Upadhyay, and K. Parekh, Phys. Rev. Lett. **96**, 127402 (2006).
[45] M. Ivey, J. Liu, Y. Zhu, and S. Cutillas, Phys. Rev. E **63**, 011403 (2000).
[46] M. Kerker, D. S. Wang, and C. L. Giles, J. Opt. Soc. Am. **73**, 765 (1983).
[47] F. A. Pinheiro, A. S. Martinez, and L. C. Sampaio, Phys. Rev. Lett. **84**, 1435 (2000).
[48] F. A. Pinheiro, A. S. Martinez, and L. C. Sampaio, Phys. Rev. Lett. **85**, 5563 (2000).
[49] B. Garcia-Camara, F. Moreno, F. Gonzalez, and J. M. Saiz, Phys. Rev. Lett. **98**, 179701 (2007).
[50] J. Liu, E. M. Lawrence, A. Wu, M. L. Ivey, G. A. Flores, K. Javier, J. Bibette, and J. Richard, Phys. Rev. Lett. **74**, 2828 (1995).
[51] Y. H. Hwang and X-L. Wu, Phys. Rev. E **49**, 3102 (1994).
[52] M. F. Islam, K. H. Lin, D. Lacoste, T. C. Lubensky, and A. G. Yodh, Phys. Rev. E **67**, 021402 (2003).
[53] J. Philip, J. M. Laskar, and B. Raj, Appl. Phys. Lett. **92**, 221911 (2008).
[54] C. P. Pang, C. T. Hsieh, and J. T. Lue, J. Phys. D **36**, 1764 (2003).
[55] R. Haghgooie and P. S. Doyle, Phys. Rev. E **75**, 061406 (2007).
[56] R. E. Rosensweig, *Ferrohydrodynamics*, 1st ed. (Dover, New York, 1997).
[57] B. Hoffmann and W. Kohler, J. Magn. Magn. Mater. **262**, 289 (2003).
[58] V. Joudrier, P. Bourdon, F. Hache, and C. Flytzanis, Appl. Phys. B: Lasers Opt. **67**, 627 (1998).
[59] C. Christiansen, Ann. Phys. **23**, 298 (1984).
[60] G. L. Fischer, R. W. Boyd, T. R. Moore, and J. E. Sipe, Opt. Lett. **21**, 1643 (1996).
[61] C. F. Bohren and D. R. Huffman, *Absorption and Scattering of Light by Small Particles* (Wiley, New York, 1983).
[62] A. C. Lind and J. M. Greenberg, J. Appl. Phys. **37**, 3195 (1966).
[63] M. Kerker, *The Scattering of Light: And Other Electromagnetic Radiation* (Academic, New York, 1969).